Systematics of a vibrational effect on the dynamic moments of inertia in superdeformed bands in the mass ≈150 region

S. Roy

Department of Nuclear and Atomic Physics, Tata Institute of Fundamental Research, Mumbai-400 005, India

An empirical semiclassical model has been proposed to investigate the nature of dynamic moment of inertia of the superdeformed (SD) bands in nuclei of mass 150 region. The model incorporates an additional frequency dependent distortion to the dynamic moment-of-inertia term akin to a vibrational component to explain the extreme spin structure of these bands. Using this model three distinct natures of the dynamic moment-of-inertia, have been identified for the SD band structure for the mass 150 region. This study establishes the role of the vibrational mode in the extreme high spin rotational structure of the atomic nuclei.

I. INTRODUCTION

Vibration and rotation are the two modes of excitation that have been observed both in atomic nuclei [1] and molecules [2]. Vibrational modes in nuclei have been observed as multipolar resonances that are collective in nature and the resonance energy exhibits a (mass number)$^{-1/3}$ dependence [3]. Low energy vibrational modes have also been observed in the nuclei, where the conjugation of the valance nucleons with the core gives rise to rotational and vibrational interplay of energy levels.

Interplay of the two modes have also been well studied in molecules through Raman and infrared spectroscopy [4], where the relative internal arrangement of the molecules can be explored. In the case of diatomic molecules, the vibration energy depends on the atomic distances between the components of the molecule and the effective interaction. Molecules with rotational and vibrational degrees of freedom, exhibit a composite spectra. If a simple scenario is considered, such as in the case of the $^{12}C - ^{16}O$ molecule, three primary types of vibrational-rotational couplings are possible, subject to the conditions $\Delta J = 0$ (Q branch), $\Delta J = 1$ (R branch), and $\Delta J = -1$ (P branch), where J is the rotational quantum number [5].

The energy of the excitation in these cases can be expressed in terms of vibrational frequency dependent moment of inertia B_ν and centrifugal distortion factor D_ν, and the angular momentum of the state I as

$$F_\nu = (B_\nu - D_\nu I(I+1))I(I+1), \tag{1}$$

where ν is the vibrational frequency.

In low-lying nuclear structure levels, the vibration and rotation couplings have been observed in many cases. When the vibration is such that it increases the deformation (β_2, γ) at constant rotational frequency, a surface distortion is observed, which evolves with time and resembles a tidal wave on the surface of the nucleus. The energy and the reduced transition probability [$B(E2)$] in this case increase with the increase of angular momentum [6,7]. Semiclassically the transition energy and the transition probability are expressed as [8]

$$E \sim aI + bI^2 + cI^3 + \dots,$$
$$B(E2) \sim \alpha I + \beta I^2 + \gamma I^3 + \dots. \tag{2}$$

Interestingly, the energy transition rate in this form assumes a variable angular momentum dependent moment of inertia. Similarly, in this work, the superdeformation phenomenon in the nuclei has been investigated and a frequency dependent effective dynamic moment of inertia has been identified which is related to a vibrational distortion. Such vibration may be thought to arise due to cluster-like structure or binary structure of nucleus at very high spin [9,10]. The effect of such a structure would be directly observed in the dynamic moment of inertia.

To date, more than 300 superdeformed (SD) bands have been observed across the nuclear landscape [11]. The superdeformation in a nucleus has been characterized as an extended ellipsoidal shape. For the ideal SD case the ellipsoidal long axis is twice the short axis in length, and corresponds to a quadrupole deformation of $\beta \sim 0.6$ [12]. Such an extended shape is stable at high spin and rotational frequency due to the interplay of collective and single particle degrees of freedom. The primary factors for the stability of shape is due to the shell corrections, which produce a local minima in the potential-energy surface, and the decrease of the Coulomb force due to larger than average separation of protons. In addition, at this high spin range ($I \geqslant 30\hbar$), the presence of highly mixed j states presents an interesting domain for theoretical studies. There has been many exhaustive theoretical studies using mean field models; Woods-Saxon [13], anharmonic oscillator potential [14,15], and Skyrme-Hartree-Fock [16]. Quite a few semiclassical macroscopic models have also been successful in presenting a good description of the SD bands [17–22].

In the superdeformation regime, the nucleus exhibits nearly a perfect quadrupole behavior with a very small regular separation in the rotational level energies. This feature may manifest as identical SD bands in neighboring nuclei [23] due to similar moment of inertia. Certain features of the moment of inertia have also been studied by the semiclassical model, where a stiff core part was identified at high spin given by [19]

$$\Im = \tfrac{3}{4}\Im_{\text{rgd}} + \tfrac{1}{4}\Im_{\text{irr}}, \tag{3}$$

where $\Im_{\text{rgd}}$ and $\Im_{\text{irr}}$, are the respective rigid-core and irrotational contribution to the total moment of inertia.

Characteristics of a rotational band can be investigated from the energy of the levels (E_L) and the angular momentum (I).

The moment of inertia ($\Im$), kinematic moment of inertia ($\Im^{(1)}$), and dynamic moment of inertia ($\Im^{(2)}$), hereafter also referred to as $\mathrm{D^{MOI}}$, are the three quantities that characterizes the evolution of the band with the spin. These are given by

$$\Im^{(1)} = I\left(\frac{dE}{dI}\right)^{-1},$$

$$\Im^{(2)} = \left(\frac{d^2E}{dI^2}\right)^{-1}. \tag{4}$$

For an ideal rotor, $\Im \equiv \Im^{(1)} \equiv \Im^{(2)}$. However, in a realistic scenario, the excited level structure in a nucleus has also been determined by the slow alignment of the pairing effect between the valance nucleons and the centrifugal stretching due to rotation [16]. Both the effects result in a $\mathrm{D^{MOI}}$ that is dependent on the rotational frequency. Both these effects can be described by the well-known semiclassical formalisms, the Harris parametrization [17] and variable moment of inertia model [18]. However, in most of the cases the SD band head is not well determined, and these two models are not adequate to determine $\mathrm{D^{MOI}}$.

Interestingly, a simple semiclassical expression between $\Im^{(1)}$ and $\Im^{(2)}$ has been derived by Wu *et al.,* [21,22]. The two parameter expression, using the Bohr Hamiltonian [24] for a well-deformed nucleus with small axial symmetry has been quite successful in describing the SD band rotational spectrum. Here the authors have quantified a constant R as a function of the angular momentum I, such that $R \equiv \sqrt{[\Im^{(1)}]^3/\Im^{(2)}}$. One can infer from this formalism that the moment of inertia can be represented in a functional form $f_n(\omega)$, $n = 1$ and $n = 2$ give $\Im^{(1)}$ and $\Im^{(2)}$, respectively. The function is given as

$$f_n(\omega) = \Im_\circ\left[1 - \frac{(\hbar\omega)^2}{a^2b}\right]^{(\frac{1}{2}-n)}, \tag{5}$$

where $\Im_\circ$ is the band-head moment of inertia, and a, and b are related with $\Im_\circ$ via

$$\Im_\circ = \frac{\hbar^2}{ab}. \tag{6}$$

The preceding two equations, (5) and (6), indicate that the there is a slow variation of $\mathrm{D^{MOI}}$ with rotational frequency. In addition, the dynamic and kinematic moment of inertia in SD bands are related to the band-head moment of inertia, $\Im_\circ$, through the two parameters and rotational frequency, ω, as the independent variable.

At this juncture, I now introduce the model primarily based on the two semiclassical scenarios mentioned previously, and the vibrational-rotational energy function, Eq. (1). In addition I also consider the experimental evidences of the octupole vibrational coupling to the SD states [25–27] and the phenomenon of fission isomers [28] that indicates a certain type of binary or cluster structure or reflection asymmetry in this type of high spin and high energy states.

The phenomenological model is chosen such that it incorporates a vibration-like distortion part and describes the slow variation of $\mathrm{D^{MOI}}$ for smooth SD bands where no sudden alignments have been observed. The function has the property such that at the band head the magnitude of the vibrational coupling is maximum and it goes to zero at the maximum observed spin ω_{max}. There are two modes of vibrational distortional coupling. When the vibrational amplitude is in the perpendicular direction to the rotation axis it increases the dynamic moment of inertia. The dynamic moment of inertia exhibits the opposite trend when the vibrational coupling is in the direction parallel to the rotation axis.

From previously mentioned energy levels of the molecular excitation [Eq. (1)], one obtains a moment of inertia term dependent on the vibrational distortion and rotational angular momentum, in the present case I propose the $\mathrm{D^{MOI}}$ as a function of rotational frequency and vibration distortion as

$$\Im^{(2)} = \Im_c^{(2)} \pm \Im_{vib}^{(2)}\left[\frac{\omega_{max} - \omega}{\omega_{max}}\right]^2, \tag{7}$$

where $\Im_c^{(2)}$ and $\Im_{vib}^{(2)}$ are, respectively, the constant and the vibration dependent part of $\mathrm{D^{MOI}}$. Parameter $\Im_{vib}^{(2)}$ is such that it describes the magnitude of the deviation of $\mathrm{D^{MOI}}$ from the perfect rotor behavior. The quantity $((\omega_{max} - \omega)/\omega_{max})^2$ is a function of rotational frequency, ω, such that at $\omega = \omega_{max}$, it goes to zero. ω_{max} is determined from the maximum observed rotational frequency of a SD band. It is assumed here that the SD band terminates at this value. Depending on the initial curvature of the experimental $\mathrm{D^{MOI}}$, the coupling between $\Im_c^{(2)}$ and $\Im_{vib}^{(2)}$ is either positive or negative. $\Im_{vib}^{(2)}$ couples positively to the constant part, if the vibration is in the plane of rotation. For the negative coupling, the vibration amplitude is more aligned towards the rotation axis, and hence decreases the magnitude of the moment of inertia.

II. FORMALISM

The atomic nucleus is a finite Fermi system. The value of the moment of inertia of the nucleus, $\Im$, lies between a rigid rotor and a liquid rotor, $\Im_{liquid} < \Im < \Im_{rgd}$. One can extract the moment of inertia parameter for a rotational band using the relation, $E_x = \frac{\hbar^2}{2\Im}I(I + 1)$. However, the average properties of a band in a nucleus are better described by the $\Im^{(1)}$ and $\mathrm{D^{MOI}}$.

Experimentally, for most of the SD bands the band-head spin is not assigned firmly, due to the missing or low intensity of the intraband linking transitions. Hence, in this work the properties of SD bands have been viewed from the $\mathrm{D^{MOI}}$ perspective, and the overall patterns in the mass region 150 are observed.

The $\mathrm{D^{MOI}}$ function is given as in Eq. (7). The function is single valued and smooth. The function has a constant part $\Im_c^{(2)}$ and a slowly varying vibrational part, parametrized through $\Im_{vib}^{(2)}[(\omega_{max} - \omega)/\omega_{max}]^2$. Using least-square fitting the two parameters of this function were extracted from the experimental $\mathrm{D^{MOI}}$ values. Then the constant part is related to the MOI of the rigid core and the variation part is similar to first term of Inglis moment of inertia $\Im_{Inglis}$ [29].

In this model the vibrational distortion effect is parametrized through the effective moment of inertia, $\Im_{vib}^{(2)}$, as a function of rotational frequency. It is noteworthy that the function exhibits a constant behavior if ω is scaled to $[(\omega_{max} - \omega)/\omega_{max}]^2$. Using Eq. (1), an approximate relation

can be inferred between $\Im_c^{(2)}$ and B_ν, as well as $\Im_{\text{vib}}^{(2)}$ and D_ν. While $\Im_c^{(2)}$ is equivalent to $1/B_\nu$, $\Im_{\text{vib}}^{(2)} \sim D_\nu [I\omega_{\max}/(\omega_{\max} - \omega)]^2$. The coupling between the two parameters $\Im_c^{(2)}$ and $\Im_{\text{vib}}^{(2)}$ is determined by the dynamics of the SD band.

III. RESULTS

The D^{MOI} [Eq. (7)] have been fitted to the experimental values using the least square minimum procedure to extract the two parameters $\Im_c^{(2)}$ and $\Im_{\text{vib}}^{(2)}$ for 23 SD bands in the mass 150 region. The extracted values are tabulated in Table I, along with the rms of the residuals for the fit, $\sum_{i=1}^{n}(\Im_i^{(2)\text{cal}} - \Im_i^{(2)\text{obs}})^2/n$, where n, $\Im^{(2)\text{cal}}$, and $\Im^{(2)\text{obs}}$, respectively, are the number of degrees of freedom, calculated value of D^{MOI}, and observed value of D^{MOI}. For each of the 23 cases shown here, the nature of the D^{MOI} in the entire rotational frequency range is well-reproduced individually.

Overall, the experimental values of the constant part to D^{MOI}, $\Im_c^{(2)}$, has a small spread, $72.3^{+15.2\%}_{-9.36\%}$, the $\Im_{\text{vib}}^{(2)}$ values span $3.7\hbar^2\,\text{MeV}^{-1}$ to $88.7\hbar^2\,\text{MeV}^{-1}$. The characteristics of D^{MOI} have been identified through the magnitude and coupling (positive or negative) of the parameters $\Im_{\text{vib}}^{(2)}$ and $\Im_c^{(2)}$.

In Figs. 1, 2, and 3, the nuclei with three distinct patterns in D^{MOI} components are plotted. Three categories of D^{MOI}, **I**, **II**, and **III**, are identified depending on the magnitude of the ratio of the D^{MOI} component, $\Im_c^{(2)}$ and $\Im_{\text{vib}}^{(2)}$, and nature of the coupling. In the category **I**, the average magnitude of $\Im_c^{(2)}$ is about eight times the average magnitude of $\Im_{\text{vib}}^{(2)}$ (Fig. 1). The

TABLE I. Fitted parameter values, $\Im_c^{(2)}$, $\Im_{\text{vib}}^{(2)}$ using Eq. (7) are tabulated.

Isotope (Band)	Category	$\Im_c^{(2)}$	$\Im_{\text{vib}}^{(2)}$	rms of residuals
^{143}Eu (SD1)	I	67.4882	5.51486	1.30959
^{143}Gd (SD)	I	68.2859	12.0957	1.00398
^{144}Gd (SD2)	I	68.2249	3.6832	0.703386
^{147}Gd (SD2)	II	65.6736	62.4044	0.515283
^{147}Tb (SD)	I	70.8534	13.7481	0.638003
^{148}Eu (SD1)	II	71.209	35.9854	0.521523
^{148}Eu (SD2)	II	71.8992	37.1367	1.07683
^{148}Gd (SD1)	II	66.3205	50.523	0.817359
^{148}Gd (SD6)	II	70.5666	70.2551	0.617295
^{149}Gd (SD1)	II	69.9208	41.7947	0.621519
^{149}Gd (SD5)	II	66.8639	52.4335	0.99385
^{149}Gd (SD6)	II	65.5212	58.6527	1.71442
^{149}Tb (SD2)	II	74.1203	16.4275	0.546993
^{150}Gd (SD5)	II	70.6088	42.7737	0.667379
^{150}Gd (SD8)	II	70.0014	49.3173	0.307386
^{150}Gd (SD9)	II	66.3469	47.9009	1.18063
^{150}Gd (SD10)	II	71.6982	56.9163	0.37468
^{150}Gd (SD12)	III	83.2367	15.7484	1.48063
^{150}Tb (SD1)	II	73.4802	17.9999	0.57067
^{151}Gd (SD3)	II	69.2381	35.52	0.594611
^{151}Tb (SD2)	III	82.8791	19.2366	1.03616
^{152}Dy (SD1)	III	82.906	16.4917	0.523973
^{153}Dy (SD3)	III	82.91	17.0606	0.812715

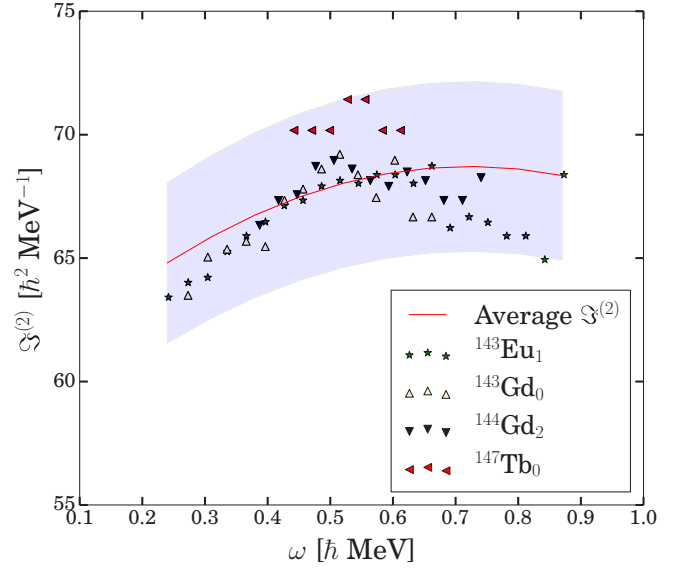FIG. 1. $\Im^{(2)}$ vs. ω for Category **I** SD bands are shown. The red line represents the average curve with the parameter value, $\Im_c^{(2)} = 68.7$ ($\hbar^2\,\text{MeV}^{-1}$) and $\Im_{\text{vib}}^{(2)} = 8.8$, respectively. The blue region spans $\pm 5\%$ of the value of the two parameters.

nuclei, ^{143}Eu, band 1, ^{143}Gd yrast SD band, ^{144}Gd band 2, and, ^{147}Tb yrast SD band, fall under this category. In this region two other SD bands, ^{150}Tb SD band 2, and ^{151}Dy SD band 1 also show a similar magnitude of the negative coupling of $\Im_{\text{vib}}^{(2)}$, but the magnitude of $\Im_c^{(2)}$ is quite higher and hence not included in the category **I**.

Thus, the region **I** is characterized by the averages $\Im_c^{(2)} = 68.7$ ($\hbar^2\,\text{MeV}^{-1}$), and $\Im_{\text{vib}}^{(2)} = 8.8$ ($\hbar^2\,\text{MeV}^{-1}$). Curiously, the coupling between the D^{MOI} component is negative, hence, the initial D^{MOI} starts with a lower value, that gradually increases and becomes equal to $\Im_c^{(2)}$ at $\omega = \omega_{\max}$. The shaded blue region in Fig. 1 corresponds to $\pm 5\%$ of the average values, depicted by the red line. All the experimental $\Im^{(2)}$ values are found to be within the region.

In category **II**, one finds 15 SD bands, where $\Im_c^{(2)}$ is about 1.5 times $\Im_{\text{vib}}^{(2)}$ and the coupling is positive like the previous category. Due to a considerable increase in the magnitude of the frequency dependent part, the initial D^{MOI} is high and decreases much more rapidly than the other two categories. The D^{MOI} components $\Im_c^{(2)}$ and $\Im_{\text{vib}}^{(2)}$ have comparable magnitude and on the average are given as 69.3 ($\hbar^2\,\text{MeV}^{-1}$) and 47 ($\hbar^2\,\text{MeV}^{-1}$), respectively.

In the final category **III** (Fig. 3), the coupling between $\Im_c^{(2)}$ and $\Im_{\text{vib}}^{(2)}$ is positive, and average values of the D^{MOI} components are $\Im_c^{(2)} = 82.98$ ($\hbar^2\,\text{MeV}^{-1}$) and $\Im_{\text{vib}}^{(2)} = 17.1$ ($\hbar^2\,\text{MeV}^{-1}$). Here, $\Im_c^{(2)}$ is higher than other two regions and about five times the average $\Im_{\text{vib}}^{(2)}$ value. As a result of the coupling the initial D^{MOI} is higher and decreases to a $\Im_c^{(2)}$ value at $\omega = \omega_{\max}$. ^{150}Gd SD band 12, ^{151}Tb SD band 2, ^{152}Dy SD band 1, and ^{153}Dy SD band 3 belong to this category. The green region represents the $\pm 5\%$ of the average values shown by the red line.
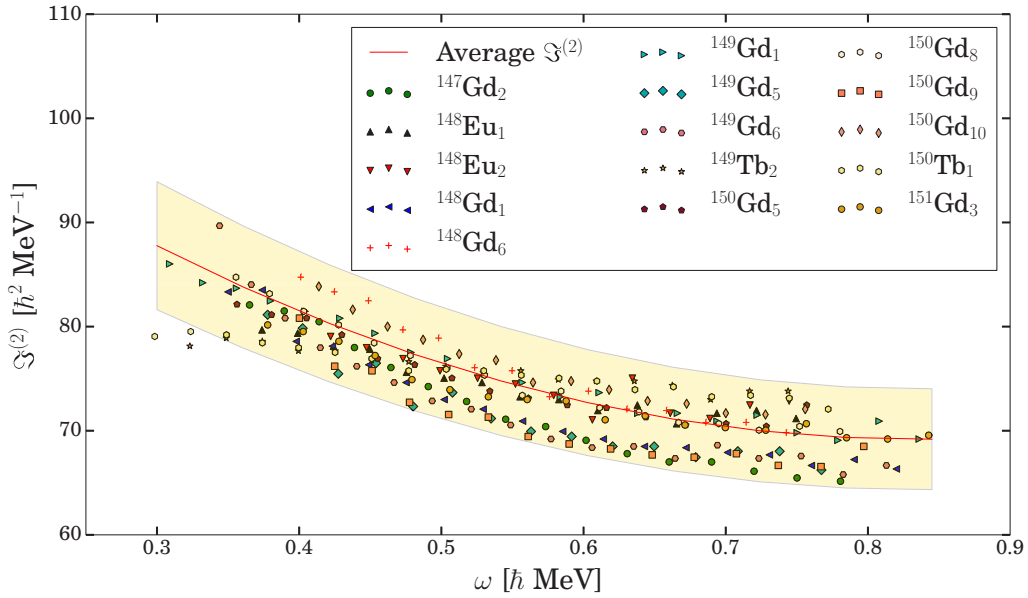
FIG. 2. $\Im^{(2)}$ vs. ω for Category **II** SD bands are shown. The red line represents the average curve with the parameter value, $\Im_c^{(2)} = 69.18$ ($\hbar^2$ MeV^{-1}) and $\Im_{\text{vib}}^{(2)} = 45.21$ ($\hbar^2$ MeV^{-1}), respectively. The yellow region spans $\pm 7\%$ of the value of the two parameters.

Thus, the three categories are given by the values:

$$\Im_c^{(2)} : \Im_{\text{vib}}^{(2)} = 68.70^{+3.43}_{-3.43} : 8.80^{+0.44}_{-0.44} \text{ Category I,}$$

$$\Im_c^{(2)} : \Im_{\text{vib}}^{(2)} = 69.18^{+4.84}_{-4.84} : 45.2^{+3.16}_{-3.16} \text{ Category II,}$$

$$\Im_c^{(2)} : \Im_{\text{vib}}^{(2)} = 82.98^{+4.14}_{-4.14} : 17.13^{+0.86}_{-0.86} \text{ Category III.}$$

It is interesting to note that $\Im_c^{(2)} \sim 68.70$, for Categories I and II are very close in magnitude, but the coupling of the $\Im_{\text{vib}}^{(2)}$ component gives rise to two different behaviors. Category

III SD bands have a different core value of $\Im_c^{(2)} = 82.98^{+4.14}_{-4.14}$ but the coupling is similar in nature to Category II. Hence, Categories II and III match at the band-head frequency, while Categories I and II match at the highest frequency ω_{max}, where $\Im_{\text{vib}}^{(2)} = 0$.

IV. SUMMARY

An empirical semiclassical two-parameter model has been used to investigate the characteristics of D$^{\text{MOI}}$ of the SD band in the mass 150 region. Using the model, three categories of D$^{\text{MOI}}$ have been identified. The D$^{\text{MOI}}$ in this model has been parametrized such that the component $\Im_c^{(2)}$ is constant and $\Im_{\text{vib}}^{(2)}$
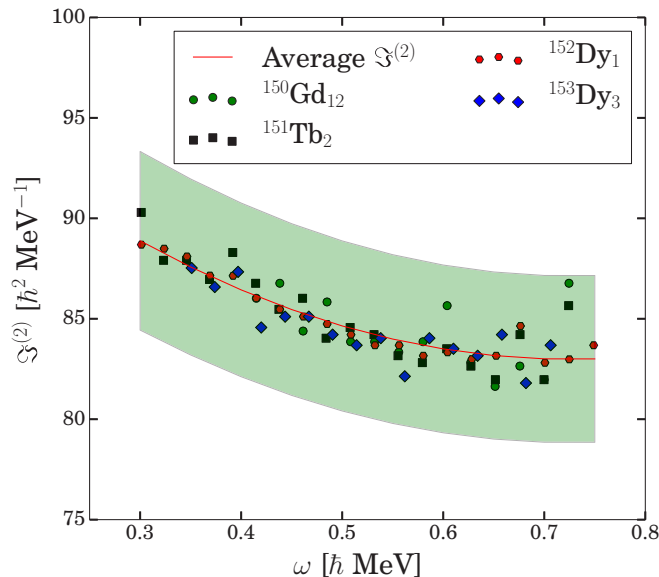

FIG. 3. $\Im^{(2)}$ vs. ω for Category **III** SD bands are shown. The red line represents the average curve with the parameter values $\Im_c^{(2)} = 82.98$ ($\hbar^2$ MeV^{-1}) and $\Im_{\text{vib}}^{(2)} = 17.13$ ($\hbar^2$ MeV^{-1}), respectively. The green region spans $\pm 5\%$ of the value of the two parameters.
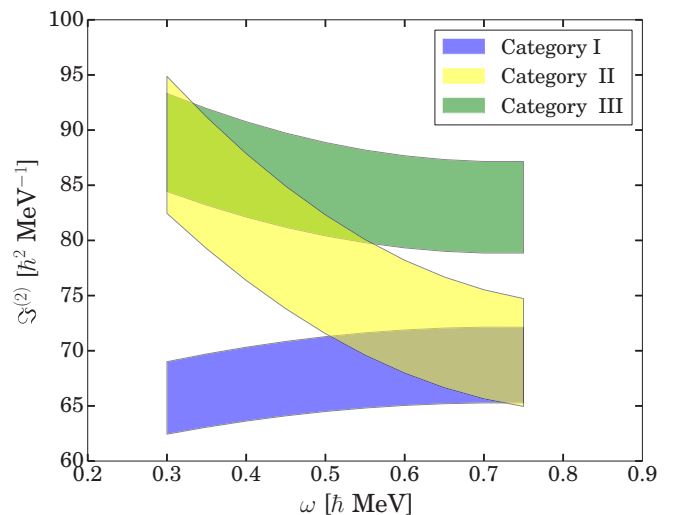

FIG. 4. The $\Im^{(2)}$ vs. ω plot shows the three regions with $\Im_c^{(2)}/\Im_{\text{vib}}^{(2)} \sim 8$ (blue), $\Im_c^{(2)}/\Im_{\text{vib}}^{(2)} \sim 5$ (green), and $\Im_c^{(2)}/\Im_{\text{vib}}^{(2)} \sim 1.5$ (yellow) for the given span of angular frequency.

is dependent on angular frequency. Experimental values, of 23 SD bands, which show a smooth behavior has been fitted using Eq. (7). In all the cases a reasonably good fit has been obtained.

The three categories of the D^{MOI} are shown for a given angular frequency range in Fig. 4. It is interesting to note that at the lower frequency limit, Categories **II** and **III**, D^{MOI} overlap. This indicates that in both scenarios, the band head D^{MOI} is similar, but the magnitude of the coupling of the vibrational component is different. At higher angular frequency, these two D^{MOI} become distinctly separate and reach the respective average rigid core values of 82.98 ($\hbar^2$ MeV^{-1}) and 69.3 ($\hbar^2$MeV^{-1}) for Categories **III** and **II**.

At the higher frequency limit, D^{MOI} in Categories, **I** and **II** overlap. While at the band head the two categories have different values, at the highest frequency ω_{max}, the band behavior merges. This shows that as the frequency increases the effect of the vibrational component diminishes and D^{MOI} merges towards the core component value of ~69.3 ($\hbar^2$ MeV^{-1}).

Thus, in this study, three distinct patterns of the D^{MOI} have been highlighted. A substantial number of SD bands have been fitted using the model and good agreement is observed between the experiment and the phenomenological model. As a result, the D^{MOI} may be thought to have a rather weak dependence on their respective nucleonic configurations. The angular frequency component, given by $[(\omega_{max} - \omega)/\omega_{max}]^2$, is a direct measure of the vibrational distortion effect and responsible for the deviation from the ideal rotor. It is natural that this model will also work for smooth SD bands in other mass regions. The present model can also be extended to calculate the $B(E2)$ rates by parametrizing the charge asymmetry through the vibrational distortion effect.

[1] A. Bohr and B. R. Mottelson, *Nuclear Structure*, Vol. I: Single-Particle Motion (World Scientific, Singapore, 1998).

[2] G. Herzberg, *Molecular Spectra and Molecular Structure: Spectra of Diatomic Molecules*, Vol. I (Van Nostrand, New York, 1950).

[3] M. N. Harakeh and A. van der Woude, *Giant Resonances: Fundamental High-Frequency Modes of Nuclear Excitation* (Oxford University Press, Oxford, 2002).

[4] N. Colthup, *Introduction to Infrared and Raman Spectroscopy* (Elsevier, New York, 2012).

[5] D. H. Rank, A. G. St Pierre, and T. A. Wiggins, J. Mol. Spectrosc. **18**, 418 (1965).

[6] S. Frauendorf, Y. Gu, and J. Sun, arXiv:0709.0254.

[7] A. D. Ayangeakaa *et al.*, Phys. Rev. Lett. **110**, 102501 (2013).

[8] A. O. Macchiavelli, A. D. Ayangeakaa, S. Frauendorf, U. Garg, and M. A. Caprio, Phys. Rev. C **90**, 047304 (2014).

[9] J.-P. Ebran *et al.*, Nature **487**, 341 (2012).

[10] C. Beck, J. Phys.: Conf. Series **569**, 012002 (2014).

[11] B. Singh *et al.*, Nucl. Data Sheets **97**, 241 (2002).

[12] P. J. Nolan and P. J. Twin, Annu. Rev. Nucl. Part. Sci. **38**, 533 (1988).

[13] J. Dudek and W. Nazarewicz, Phys. Rev. C **31**, 298 (1985).

[14] I. Ragnarsson, Nucl. Phys. A **347**, 287 (1980).

[15] R. Bengtsson, Phys. Scr. **24**, 200 (1981).

[16] W. Satuła, J. Dobaczewski, J. Dudek, and W. Nazarewicz, Phys. Rev. Lett. **77**, 5182 (1996).

[17] S. M. Harris, Phys. Rev. **138**, B509 (1965).

[18] M. A. J. Mariscotti, G. Scharaff-Goldhaber, and B. Buck, Phys. Rev. **178**, 1864 (1969).

[19] W. J. Swiatecki, Phys. Rev. Lett. **58**, 1184 (1987).

[20] J. L. Wood, and R. W. Fink, Nucl. Phys. A **224**, 589 (1974).

[21] C. S. Wu, J. Y. Zeng, Z. Xing, X. Q. Chen, and J. Meng, Phys. Rev. C **45**, 261 (1992).

[22] C. S. Wu, L. Cheng, C. Z. Lin, and J. Y. Zeng, Phys. Rev. C **45**, 2507 (1992).

[23] C. Baktash, B. Haas, and W. Nazarewicz, Annu. Rev. Nucl. Part. Sci. **45**, 485 (1995).

[24] A. Bohr and B. R. Mottelson, *Nuclear Structure*, Vol. II: Nuclear Deformations (World Scientific, Singapore, 1998).

[25] S. Bouneau *et al.*, Z. Phys. A **358**, 179 (1997).

[26] D. Roßbach *et al.*, Phys. Lett. B **513**, 9 (2001).

[27] A. Prevost *et al.*, Eur. Phys. J. A **10**, 13 (2001).

[28] J. Schirmer, J. Gerl, D. Habs, and D. Schwalm, Phys. Rev. Lett. **63**, 2196 (1989).

[29] D. R. Inglis, Phys. Rev. **103**, 1786 (1956).